Lithogenic hydrogen supports microbial primary production in subglacial and proglacial environments

Eric C. Dunham[a], John E. Dore[b], Mark L. Skidmore[c], Eric E. Roden[d], and Eric S. Boyd[a,1]

[a]Department of Microbiology and Immunology, Montana State University, Bozeman, MT 59717; [b]Department of Land Resources and Environmental Sciences, Montana State University, Bozeman, MT 59717; [c]Department of Earth Sciences, Montana State University, Bozeman, MT 59717; and [d]Department of Geoscience, University of Wisconsin–Madison, Madison, WI 53706

Edited by Donald E. Canfield, Institute of Biology and Nordic Center for Earth Evolution, University of Southern Denmark, Odense M., Denmark, and approved November 11, 2020 (received for review April 15, 2020)

Life in environments devoid of photosynthesis, such as on early Earth or in contemporary dark subsurface ecosystems, is supported by chemical energy. How, when, and where chemical nutrients released from the geosphere fuel chemosynthetic biospheres is fundamental to understanding the distribution and diversity of life, both today and in the geologic past. Hydrogen (H_2) is a potent reductant that can be generated when water interacts with reactive components of mineral surfaces such as silicate radicals and ferrous iron. Such reactive mineral surfaces are continually generated by physical comminution of bedrock by glaciers. Here, we show that dissolved H_2 concentrations in meltwaters from an iron and silicate mineral-rich basaltic glacial catchment were an order of magnitude higher than those from a carbonate-dominated catchment. Consistent with higher H_2 abundance, sediment microbial communities from the basaltic catchment exhibited significantly shorter lag times and faster rates of net H_2 oxidation and dark carbon dioxide (CO_2) fixation than those from the carbonate catchment, indicating adaptation to use H_2 as a reductant in basaltic catchments. An enrichment culture of basaltic sediments provided with H_2, CO_2, and ferric iron produced a chemolithoautotrophic population related to *Rhodoferax ferrireducens* with a metabolism previously thought to be restricted to (hyper) thermophiles and acidophiles. These findings point to the importance of physical and chemical weathering processes in generating nutrients that support chemosynthetic primary production. Furthermore, they show that differences in bedrock mineral composition can influence the supplies of nutrients like H_2 and, in turn, the diversity, abundance, and activity of microbial inhabitants.

hydrogen | basalt | carbonate | chemoautotrophy | iron reduction

Subglacial and proglacial environments host abundant, diverse, and active microbiomes supported by combinations of nutrients derived from relict organic matter, minerals, and the interaction of water and minerals (1–5). In catchments containing abundant sedimentary carbonates and shales, the biological oxidation of pyrite (FeS_2) has been suggested to be a primary control on the composition of subglacial sediment microbiomes (5–7), likely due to its potential role in supplying reductant to drive primary production (8). Far less is known of the nutrients that support communities inhabiting subglacial and proglacial systems overlaying silicate (e.g., granite, gneiss, basalt) bedrock. This is a major knowledge gap considering that silicate-based glaciers are prevalent habitat types on Earth both today and in the geological past (2, 9) and potentially on other icy planetary bodies such as Saturn's moon Enceladus (10).

Hydrogen (H_2) is a common metabolic substrate in many rock-hosted ecosystems (11–14), including subglacial environments (15, 16). H_2 can be generated abiotically through the reduction of water by ferrous iron minerals (17, 18), the radiolysis of water (13), or the activity of one of several classes of microbial enzymes (19, 20). In addition, H_2 can be produced through silica radical-based mechanisms (21), which have recently been suggested to be of importance in generating H_2 in cold (~0 °C), dark subglacial ecosystems (15, 16, 22). In this process, mechanical shearing of silicates is proposed to generate surface radicals that, when exposed to water, produce H_2 through reactions **1** and **2**:

$$Si^{\bullet} + H_2O \rightarrow SiOH + H^{\bullet}, \quad [1]$$

$$H^{\bullet} + H^{\bullet} \rightarrow H_2. \quad [2]$$

Moreover, this mechanism may help to explain why abundant members of microbial communities in various subglacial ecosystems appear to be dependent on H_2 as an electron donor in the absence of evidence for other known biotic or abiotic pathways for H_2 production (3, 15, 23–26).

H_2 may be expected to be an even more important electron donor supporting primary production in mafic (basaltic) subglacial and proglacial systems when compared to those underlain by felsic (granitic) or carbonate bedrock. In addition to containing abundant silicates, basalts are typically enriched in iron [8–13% by weight, (27)]. The iron in basalts has been linked to production of H_2 from water in subsurface ecosystems in the Columbia River (CR) basin, Washington, United States (18). For example, in laboratory experiments containing anoxic water buffered at pH 6.0, H_2 production from crushed CR basalt was 4.1 and 5.5 nmol·g^{-1}·d^{-1} at 30 and 60 °C, respectively. When water–rock reactions were buffered at pH 7.0, rates decreased to 2.4 and 2.9 nmol H_2·g^{-1}·d^{-1} at 30 and 60 °C, respectively. Assuming Arrhenius kinetics, an extrapolation of these rates to temperatures relevant to glacial meltwaters (~0 °C) yields anticipated H_2 production rates of 2.8 and

Significance

In the absence of light, biomass production is driven by chemical energy through microbial chemosynthesis. H_2, a potent reductant capable of supporting chemosynthesis, is readily generated by reactions between iron and silicate minerals and water. Here, we show that lithogenic H_2 produced by glacial comminution of iron- and silica-rich basaltic bedrock supports microbial chemosynthesis. Lithogenic production of H_2 in cold, dark subglacial environments and its use to generate chemosynthetic biomass suggest the potential for subglacial habitats to serve as refugia for microbial communities in the absence of sunlight, such as during Snowball Earth episodes or on icy planets where photosynthesis may not yet have evolved or where light is restricted.

Author contributions: E.C.D. and E.S.B. designed research; E.C.D. performed research; M.L.S. contributed new reagents/analytic tools; E.C.D., J.E.D., E.E.R., and E.S.B. analyzed data; and E.C.D. and E.S.B. wrote the paper.

The authors declare no competing interest.

This article is a PNAS Direct Submission.

[1]To whom correspondence may be addressed. Email: eboyd@montana.edu.

This article contains supporting information online at https://www.pnas.org/lookup/suppl/doi:10.1073/pnas.2007051117/-/DCSupplemental.

Published December 21, 2020.

2.0 nmol·g^{-1}·d^{-1} at pH 6.0 and 7.0, respectively. These rates are similar to those (~5 nmol H_2·g^{-1}·d^{-1}) obtained in crushing experiments using a variety of silicate minerals incubated at 0 °C (15, 16). Thus, glaciers overriding basaltic bedrock might be expected to generate H_2 via either the silica radical- or iron-based mechanisms—or both—which may in turn support more abundant and active hydrogenotrophic communities than those in carbonate-hosted subglacial systems.

Here, we examine the role of H_2 in supporting microbial communities in proglacial and subglacial sediments collected from contrasting basaltic and carbonate/shale catchments: Kötlujökull, Iceland (KJ), and Robertson Glacier, Alberta, Canada (RG), respectively. These sediments, collected beneath or near the terminus of each glacier, represent recently exposed subglacial material generated by glacial comminution. Furthermore, the microbial communities they host are likely seeded by and highly reflective of those existing in the subglacial environments of their host catchments, as has been reported previously (4, 6). We hypothesized that H_2 would be elevated in meltwaters and/or sediment porewaters from the former when compared to the latter. In turn, we hypothesized that the abundance and activity of hydrogenotrophic autotrophs would be higher in the basaltic system due to selection for such organisms during the assembly of those communities. Our results are discussed in consideration of the role of bedrock type in supporting H_2-dependent primary production in diverse subglacial and proglacial sediment habitats in contemporary and past environments on Earth and in subglacial habitats on extraterrestrial icy planetary bodies such as Enceladus.

Materials and Methods

Field Site Descriptions. KJ (63°36′N, 18°52′W) drains the southeast flank of Mýrdalsjökull, a temperate ice cap in southern Iceland atop Katla volcano, and is the largest outlet on its east side. As of 1997, the glacier ranged in elevation from 1,200 to 220 m over a length of 15 km, with its terminal ice front stretching nearly 12 km on a flat outwash plain known as Mýrdalssandur (28). The bedrock beneath KJ consists primarily of Upper Pleistocene-aged hyaloclastites, pillow lava, and associated basaltic sediments (29). The iron and silica content of the basaltic and rhyolitic rock in the Katla volcanic system range from ~4 to 17% and 46 to 74% by weight, respectively (30).

RG (50°44′N, 115°20′W) drains the northern flank of the Haig Icefield in Peter Lougheed Provincial Park, Kananaskis Country, Alberta, Canada. The bedrock in this catchment is of Upper Devonian age and consists of impure limestones, dolostones, and dolomitic limestones with interbeds of shale, siltstone, and sandstone (31, 32). Sediments from RG consist of 25 to 56% carbonate with the balance potassium feldspar (20 to 49%), quartz (18 to 25%), muscovite (0.5 to 3%), and pyrite (0 to 1%) (33). As of 2011, the glacier spanned an elevational gradient of 2,900 to 2,370 m with a length of ~2 km, terminating on a flat till plain.

Sample Collection and Field-Based Analyses. At KJ, dangerously high water levels on 11 October 2016 dictated that water and sediments be collected from the Múlakvisl meltwater stream at a proglacial location (63°32.099′N, 18°50.421′W) ~1 km downstream from the glacier terminus. Saturated sediments were collected from the stream bank using a flame-sterilized stainless-steel spoon and were placed into sterile 500-mL jars. Sediments were frozen on site with dry ice and maintained at −20 °C during transport to and storage at Montana State University. Saturated sediments from RG were collected from an ice cave at the terminus of the glacier on 14 September 2009, as reported previously (8), and are subglacial in nature given the sampling location beneath the glacier. At both sample locations, the surface layer (1 cm) of sediments was removed before samples were collected and preserved for analyses.

Electrical conductivity (EC) and pH were measured using a SevenGo Duo pro pH/Ion/Conductivity probe (Mettler Toledo). Meltwaters were collected with a syringe and were immediately transferred to clean glass serum vials, stoppered and crimp sealed, and then subjected to dissolved oxygen and alkalinity titrations within 5 h of sampling. Samples were allowed to equilibrate to ambient temperature in sealed vials prior to taking measurements. Dissolved oxygen was measured using a Mettler Toledo OptiOx probe. Total alkalinity was determined using a Hach digital titrator to titrate samples with 1.6 N sulfuric acid to an endpoint pH of 4.5. The pH was monitored using a SevenGo Duo pro pH/Ion/Cond probe.

Total sulfide was determined using the methylene blue reduction method (34). KJ meltwater was filtered through a 0.2-μm nylon membrane button filter directly into assay reagents in the field. Assay tubes were then wrapped in aluminum foil and subjected to absorbance analyses at the laboratory within 1 wk of collection using a Genesys 10S Vis spectrophotometer (Thermo Scientific) and a wavelength of 670 nm. Samples for determining concentrations of dissolved gases other than sulfide (H_2, CH_4, and CO_2) were collected using a modified bubble-strip method, as described previously (35). Briefly, a 60-mL Luer-lock syringe was filled with 20 mL of N_2 gas. Twenty milliliters of KJ meltwater were then introduced into the syringe followed by vigorous shaking for 1 min to allow for gas equilibration. The gas bubbles were then transferred to glass vials containing a saturated sodium chloride solution for storage until analysis by gas chromatography, as previously described (36).

Total Organic Carbon and Total Nitrogen Determinations. KJ and RG sediment samples were dried overnight at 80 °C, then hand milled in an acid-washed (overnight in 10% HNO_3) porcelain mortar and pestle and sieved to 63 μm. Triplicate subsamples were acidified with 2 N HCl in silver foil cups until acid addition did not induce bubbling during a 2-h incubation. Acidified subsamples were then washed twice with diH_2O and dried for 24 h at 80 °C after each wash. Triplicate acidified (Ag foil-wrapped) and triplicate unacidified samples were then wrapped in tin foil and analyzed on a Costech ECS 4010 (Costech Analytical Technologies) equipped for carbon and nitrogen analyses using a combustion temperature of 980 °C, a reducing oven temperature of 650 °C, a gas chromatography (GC) oven temperature of 65 °C, and a 4-m length GC column. External acetanilide standards were used to create C and N calibration curves. Total organic carbon (TOC) was determined as the difference between total carbon in unacidified and acidified samples.

Most Probable Number Assay Preparation. Most probable number (MPN) assays were conducted to determine the abundance of cultivatable cells associated with RG and KJ glacial sediments capable of coupling H_2 oxidation to autotrophic growth. Clean, acid-washed (overnight with 5% HNO_3) 24-mL serum vials were filled with 9 mL of M9 minimal medium (37) with the following modifications: The concentration of $MgSO_4$ was reduced to 200 μM and carbon sources were omitted. Medium was deoxygenated by purging with 0.2-μm nylon filter-sterilized nitrogen (N_2) gas passed over heated (210 °C) and H_2-reduced copper shavings. The headspace of vials was flushed with H_2 for 5 min and then CO_2 was added to achieve a final headspace mixing ratio of 80% H_2 and 20% CO_2. Oxidants, including Na_2SO_4, the ferric iron-containing minerals hematite and ferrihydrite, and $NaNO_3$ were prepared in sterile anoxic M9 salts medium and added to a final concentration of 1 mM. Hematite particles (<5 μm) were purchased from Sigma-Aldrich. Ferrihydrite was synthesized as previously described (38). For aerobic MPNs, 16 mL (at ambient pressure) filter-sterilized air was added to each vial via syringe. Anoxic and filter-sterilized Wolfe's vitamins and SL-10 trace elements solutions (37) were added to each bottle to final dilutions of 1 mL·L^{-1}.

Glacial sediments were thawed overnight at 4 °C and 5 g of thawed sediment (wet weight) were added to 27 mL of autoclaved and cooled M9 salts to generate a ~1:10 (vol/vol) sediment slurry. Vials were sealed and deoxygenated as described above and were kept on ice during all manipulations. Serial 1:10 dilutions of this slurry (initial dilution factor, 10^1) were made in sterile, anoxic M9 medium out to a sediment dilution factor of 10^7. Finally, MPN series were inoculated in triplicate by transfer of 1 mL of the appropriate sediment dilution to each experimental vial. Three abiotic control vials were prepared for each condition. These were autoclaved for 30 min at 121 °C, incubated for 24 h at 4 °C to allow for germination of spores, and reautoclaved. All vials were incubated at 4 °C.

MPN Assessment Using DNA Evidence. Following 6 mo of incubation, MPN vials were qualitatively judged to be positive or negative for growth by measuring the amount of extractable DNA in each microcosm. Two milliliters of culture were removed from each MPN assay microcosm and were concentrated by centrifugation (14,000 × *g*, 15 min, 4 °C). Pellets were overlain with 400 μL of CTAB buffer and 200 μL of a 500 mg·L^{-1} molecular-grade skim milk solution (Hardy Diagnostics) and DNA was then extracted following the CTAB S protocol (39). DNA was resuspended in 50 μL of molecular-grade H_2O and the concentration was determined with the Qubit dsDNA HS Assay kit and fluorometer (Molecular Probes).

Microcosms were determined to be positive for growth if >2 ng of DNA was recovered from a 2-mL culture sample. This amount of DNA was empirically determined to be associated with the growth of cells in MPN vials based on recovery of ≤1 ng·mL^{-1} in autoclave killed controls. Microcosms were assayed until all three microcosms in two sequential serial dilutions had

been judged negative. Then the pattern of positive and negative growth across three serial dilutions, along with the sediment dilution factors associated with those microcosms, was used to estimate the MPN of cells capable of growth under the provided enrichment conditions present in each gram of proglacial or subglacial sediment inoculum. Selection of three appropriate serial dilutions, proper accounting for sediment dilution factor, and the tables used in estimating MPN are described in the US Food and Drug Administration's *Bacteriological Analytical Manual* (40).

MPN Assessment Using Metabolic Evidence. Metabolic activity assays were used in parallel with DNA extractions to generate MPN estimates correlated with the use of experimentally supplied oxidants. In microcosms with CO_2 only, acetate and methane were measured. Sulfide was assayed in microcosms amended with sulfate. Ferrous iron was measured in hematite- and ferrihydrite-amended microcosms and nitrite was assayed in microcosms amended with nitrate. Microcosms were judged to be positive if the concentration of the assayed metabolite was 3 standard deviations (SDs) higher than its average concentration in three killed controls. MPN was then estimated from the pattern of positive and negative microcosms as described above.

Production of acetate was determined using a 1-mL culture sample via ion chromatography using a Metrohm 930 Compact IC Flex ion chromatograph (Metrohm) equipped with a 25-mm Metrosep A Supp 5 anion column and 930 Compact IC Flex 1 conductivity detector. Column oven temperature was set to 40 °C. A 3.2 mM Na_2CO_3 plus 1 mM $NaHCO_3$ solution was used as eluent at a flow rate of 0.7 mL·min^{-1}. The lower limit of acetate detection, as determined by standard curves, was 2.4 μM. Production of methane was determined from a 1-mL headspace sample via gas chromatograph as described previously (36). Production of sulfide was determined from a 0.75-mL culture sample using the methylene blue reduction method (34). Production of soluble or particulate ferrous iron was determined in a 0.5-mL culture sample using the ferrozine method (41). To prevent oxidation, samples were immediately acidified by addition of HCl to a final concentration of 0.5 M. Production of nitrite was determined in a 1-mL culture sample using a Griess assay modified as described previously (42).

MPN (Meta)genome Sequencing. Total genomic DNA from select MPN microcosms was subjected to Illumina library preparation and paired-end sequencing (2 × 150 bp) with the NovaSeq platform at the Genomics Core Facility at the University of Wisconsin–Madison. Sequences were assembled, binned, and annotated as previously described (43) (detailed in *SI Appendix*). Manual BLASTp searches were conducted to search for specific proteins involved in CO_2 fixation pathways, dissimilatory sulfate reduction, dissimilatory nitrate reduction, putative ferric iron reduction pathways, and reversible H_2 oxidation (i.e., [NiFe]- and [FeFe]-hydrogenases). BLAST searches were conducted using bait sequences specific to the subunits harboring the active site as well as requisite accessory subunits of each protein complex of interest. Matches with an E value $<1 \times 10^{-6}$, >30% amino acid homology, and covering >60% of the length of the BLASTp bait sequence were considered positive hits. Hits were further screened based on the presence of amino acid residues unique to select functional genes, e.g., the conserved cysteinyl residues demarcating [NiFe]-hydrogenases from membrane bound oxidoreductases (Mbx, Nuo) (44). Putative [NiFe]- and [FeFe]-hydrogenases were confirmed and classified using the HydDB tool (45). The assembled metagenomic data are available under National Center for Biotechnology Information (NCBI) BioProject ID PRJNA622799.

H_2 Oxidation Assays. H_2 oxidation assays were conducted in acid-washed 160-mL serum vials prepared as described above for MPN assays. Vials were filled with artificial Skálm Pore Water (SPW) medium (for KJ sediment samples) or artificial RG Pore Water (RGPW) medium (for RG sediment samples) made in milliQ H_2O. The composition of SPW was derived from a previous geochemical analysis of the Skálm River, an outlet of KJ to the north of Múlakvisl (46). The composition of this medium is as follows: SiO_2 (500 μM), NaCl (500 μM), KCl (25 μM), $CaCl_2$ (250 μM), and $MgCl_2$ (150 μM). The pH of the medium was adjusted to 6.8 with 1 M NaOH. RGPW medium composition was derived from geochemical analysis of RG outflow waters and has been described previously (47). Serum bottles were filled with 60 mL of SPW or RGPW medium for uninoculated controls or 48 mL for heat-killed sediment controls and experimental vials. Vials containing medium were autoclaved and then cooled to 4 °C. Twenty grams of sediment (wet weight) were added to each vial except for uninoculated controls, followed immediately by stoppering and deoxygenation with N_2 on ice as described above. Assays to measure rates of H_2 transformation under aerobic conditions were not subjected to deoxygenation. Heat-killed sediment controls were autoclaved twice after inoculation as described above.

Twenty-five milliliters of headspace gas was removed from each microcosm and replaced with filter-sterilized CO_2 to achieve a final headspace mixing ratio of 20%. Oxidant solutions (prepared in sterile anoxic SPW or RGPW medium using salts described above) were added to microcosms to achieve a final concentration of 1 mM. The uninoculated and heat-killed controls had the same headspace and medium composition as the CO_2-amended rate assays, with extra medium added to uninoculated microcosms to account for the lack of sediment. Finally, H_2 was added to a final headspace mixing ratio of 500 ppmv (~1.7 μmol H_2 per microcosm). Vials were incubated at 4 °C upside-down to minimize potential H_2 diffusion through stoppers.

The headspace mixing ratio of H_2 was monitored over time via gas chromatography. For subsampling, 1 mL of ultrapure N_2 gas was added to microcosm headspace and mixed well. One milliliter of the mixed headspace was then removed and diluted 1:4 with ultrapure N_2. Gases were allowed to equilibrate and the concentration of H_2 was determined as previously described (36). Gas phase concentrations were converted to dissolved aqueous phase concentrations according to Henry's law, as previously described (11). Total microcosm H_2 content was calculated as the sum of headspace and aqueous phase H_2. The maximum rate of net H_2 oxidation was calculated by applying linear regressions to subsets of each data series, as indicated in *SI Appendix*, Tables S1 and S2. The inverse of the slope of each regression, as presented in *SI Appendix*, Table S3, was taken to be the rate of net H_2 oxidation. Following termination of the incubation, microcosms were assayed for concentrations of total ferrous iron (soluble and particulate), acetate, and methane, as described above.

CO_2 Fixation Assays. Rates of CO_2 fixation were determined using previously described methods (8). Briefly, acid-washed 160-mL serum vials were filled with 55 mL of SPW or RGPW medium and autoclaved before inoculation with 10 g wet weight of KJ or RG sediments, respectively. After inoculation, microcosms were amended with oxidant solutions/suspensions to achieve a final concentration of 1 mM, as described above. Inoculated microcosms were purged with N_2 gas as described above. The headspace of microcosms was then flushed with filter-sterilized H_2 gas. For oxic microcosms, 33 mL each of filter-sterilized air and CO_2 were added to the headspace and mixed before 66 mL of mixed gas were removed, leaving 100 mL of headspace comprising 60% H_2, 20% air, and 20% CO_2. In all other microcosms, 25 mL of filter-sterilized CO_2 were added and mixed before 25 mL of mixed gas were removed, for final headspace composition of 80% H_2 and 20% CO_2. Heat-killed controls were prepared by double-autoclaving as described above. Assays were initiated by the addition of 5 μCi of $NaH^{14}CO_3$.

The amount of ^{14}C incorporated into biomass was determined by uniformly resuspending sediments and removing a 1-mL subsample aseptically using an N_2-purged and sterile syringe and needle. Subsamples were acidified to pH <2 by addition of 12 N HCl, vortexed, and allowed to vent in a fume hood for 1 h to volatilize and off-gas unreacted $NaH^{14}CO_3$. Samples were then spun down for 10 min at 17,000 × *g* and supernatant was removed. Pellets were washed three times by adding 1 mL of 0.1 M HCl, vortexing, and spinning down as described above. Finally, washed pellets were resuspended in 1 mL of milliQ water, transferred to scintillation vials, and mixed with 10 mL of CytoScint Liquid Scintillation Cocktail (MP Biomedicals). The radioactivity associated with each sample was then quantified with a Tri-Carb 2900TR liquid scintillation counter (PerkinElmer).

A standard curve was constructed to account for quenching of photons by sediments suspended in the scintillation cocktail. Microcosms not spiked with ^{14}C were prepared and subsamples were processed as described above. $NaH^{14}CO_3$ was then added in the amount of 40, 70, and 200 pCi per scintillation vial. Triplicate subsamples were prepared at each ^{14}C activity for vials that contained sediments and those that did not, and activity was counted by liquid scintillation as described above.

To determine the amount of CO_2 fixed in each microcosm, the following calculations were used. Radioactivity measured in disintegrations per minute was converted to microcuries and activity in microcuries was corrected for sediment quenching using the curve described above. Carbon uptake (C_{uptake}) was calculated using Eq. **3** below, where DIC is the sum of inorganic carbon added to each microcosm and present in growth medium, A_{POC} is the measured activity of sample particulate organic carbon, and A_{DIC} is the activity of the $H^{14}CO_3^-$ spike added to each microcosm:

$$C_{uptake} = \frac{DIC \times A_{POC}}{A_{DIC}}. \quad [3]$$

Results were normalized to grams dry weight sediment (gdws) and the means and SDs of measurements on triplicate microcosms are reported. Rates of microbial carbon fixation were determined by applying linear regressions to subsets of the C_{uptake} datasets presented in *SI Appendix*, Tables S4 and S5. The slopes of these regressions are presented in *SI Appendix*, Table S6 and were taken to be the maximum rates of carbon fixation.

Inoculation and Monitoring of Transfer Cultures. MPN cultures inoculated with KJ sediments and amended with hematite were transferred at a 1:10 (vol/vol) ratio into fresh microcosms (70-mL serum bottles, 30 mL of M9 medium prepared and amended as described above for MPN assays). Production of cells was monitored by filtering cells onto 0.22-μm black polycarbonate filters (MilliporeSigma), staining cells with SYBR Gold nucleic acid gel stain (Life Technologies) at a final dilution factor of 10,000, and enumeration via epifluorescence microscopy using an Evos FL microscope (Life Technologies).

Results and Discussion

Sources of H_2 in Glacial Meltwaters. The concentration of dissolved H_2 in the outflow stream of KJ, a basalt hosted glacier in southern Iceland, was 426.8 ± 248.2 nM (n = 3) in October 2016 (~1 km from glacier terminus). The variability in the H_2 measurement may be due to the highly turbulent nature of the stream flow at the time of sampling. At RG, a carbonate-hosted system in southern Alberta, Canada, the concentration of H_2 in meltwater sampled from the terminus of the glacier was 41.6 nM in October 2014 (48). Unfortunately, the variability associated with this measurement cannot be assessed due to the lack of replicate samples. Other measured geochemical parameters are reported in Table 1.

The concentration of H_2 measured in KJ meltwaters was similar to or in excess of concentrations measured in waters typically thought of as being enriched in H_2, including high-temperature volcanic influenced hot spring systems where dissolved H_2 concentrations rarely exceed 1 μM (11, 12). Given that KJ drains Katla Volcano, it cannot be ruled out that the H_2 detected in the meltwaters may be volcanic in origin. However, unlike KJ waters, whose low conductivities (82 μS/cm) are consistent with a meteoric origin, waters influenced by volcanic input tend to have much higher conductivities [average >1,700 μS/cm (49)]. This observation, combined with the ~15-km distance between the KJ sampling location and the primary vent of Katla Volcano, suggests that other sources are likely contributing H_2 to meltwaters at KJ leading to the high concentrations measured. However, without knowing the precise conduits emanating from the volcano and their proximity to KJ, a hydrothermal source for H_2 in meltwaters cannot be excluded.

Previous studies have shown that pulverization of silicate minerals followed by exposure to water can generate H_2 at temperatures ranging from ~0 to 35 °C (15). Based on the detection of silica radicals following mineral pulverization, a cataclastic mechanism of H_2 generation was proposed [i.e., reactions **1** and **2** (15)]. Furthermore, it was suggested that this cataclastic mechanism mimics the process of glacial comminution of silicate bedrock (15) and thus could explain the unusually high H_2 concentrations detected in meltwaters from several subglacial habitats (23). However, this study only accounted for gas that was generated upon exposure of pulverized minerals to water and thus excluded the potential for gas to be released from rock inclusions during mechanical crushing. More recent studies have shown that fluid inclusions in muddy carbonates and shales (including those sampled from RG) contain H_2 that is released during rock crushing (16) and could be responsible for the H_2 detected in RG meltwaters.

The minerology of basalts and other mafic rocks makes possible another H_2-generating mechanism: the reduction of water by ferrous silicates, as proposed for the Columbia River Basalt group of central Washington (18). This mechanism might be enhanced in subglacial systems that are actively exposing fresh iron-bearing minerals (e.g., fayalite) capable of reacting with water. Importantly, like muddy carbonates and shales, fluid inclusions in basalts have also been shown to contain H_2 that is suggested to derive from iron-based reduction of water when the basalts were crystalizing at high temperature (>400 °C) (50). Thus, glacial comminution or fracturing of the host basalt bedrock could expose fresh iron and silicate minerals capable of reacting with water and producing H_2 via mechanisms described above or could release H_2 from fluid inclusions.

Regardless of the relative contributions of each of these mechanisms to the availability of H_2 in subglacial and proglacial systems, Icelandic volcanic rocks, being enriched in both silica and iron (27, 30, 51) relative to carbonates/shales such as those dominating the RG catchment (33), may thus be predicted to generate more H_2 during glacial comminution. Our field data support this prediction, with an order of magnitude more dissolved H_2 measured in the meltwaters of KJ than in those of RG. Importantly, the dissolved H_2 measured in meltwaters from both systems was higher than would be expected based on equilibration with atmospheric H_2 alone [<0.5 nM, given an atmospheric concentration of ~500 parts per billion (52)], consistent with a source for H_2 in the glacial bedrock/sediments as described above. Furthermore, H_2 at concentrations even lower than those measured in KJ or RG meltwaters has been shown to support biological H_2 oxidation in other systems (53), and H_2 oxidizing microbial populations have been recently reported in subglacial ecosystems in Antarctica (26). Together, these observations suggest the potential for H_2 oxidation to support microbial life in both KJ and RG sediment communities.

An additional question concerns the source of oxidants capable of supporting H_2-dependent growth in subglacial habitats. The generation of H_2 due to reduction of water by either cataclastic silica radical- or ferrous iron-based reactions must achieve charge/redox balance, which should occur via an accompanying oxidation reaction. In the case of silica-radical–based reduction of water, it has been suggested that hydroxyl radicals are formed and that these can oxidize ferrous iron or sulfide in bedrock minerals, leading to formation of ferric iron or sulfate (16). Likewise, reduction of water by ferrous iron in minerals is accompanied by iron oxidation to yield ferric iron (18, 50). In subglacial systems, constant flow of ice and meltwater along with comminution of underlying bedrock could transport both H_2 (however produced) and oxidized minerals downstream (54) to environments with geochemical conditions that are favorable for the reverse of these reactions to occur.

Table 1. Geochemical measurements for glacial meltwaters and sediments from Kötlujökull, Iceland, and Robertson Glacier, Alberta, Canada

Sample site	pH	EC, μS/cm	DO, ppm	Fe^{2+}, mg/L	S^{2-}, μM	H_2, nM	CH_4, nM	CO_2, μM	DIC, μM	TOC, mg·gdws^{-1}	TN, μg·gdws^{-1}
Kötlujökull	6.8	82.1	10.3	ND	3.00	426.8 (248.2)	1.1 (0.1)	77.3 (50.2)	ND	0.38 (0.14)	BLD
Robertson	8.8*	32.5*	11.3*	0.05†	0.31†	41.6†	10.8†	ND	603‡	24.8 (14.0)	212.7 (54.2)

SDs of triplicate analyses are denoted in parentheses, where available. The limit of detection for nitrogen, given the instrumentation and techniques used, was 27 μg·gdws^{-1}. Abbreviations: BLD, below limit of detection; DIC, dissolved inorganic carbon; DO, dissolved oxygen; EC, electrical conductivity; gdws, gram dry weight sediment; ND, not determined; TN, total nitrogen; TOC, total organic carbon.

*Data from Boyd et al. (47).

†Data from Canovas (48).

‡Data from Boyd et al. (8).

Rates of Net H_2 Oxidation. To begin to assess the role of H_2 in supporting microbial life in subglacial and proglacial habitats, potential rates of net H_2 oxidation were determined in microcosm assays amended with H_2 and CO_2 with or without one of several common oxidants, including SO_4^{2-}, hematite, ferrihydrite, NO_3^-, and O_2 (Fig. 1 *A* and *C*). In microcosms prepared without sediments (uninoculated) or with autoclaved sediments (heat killed), net H_2 loss was equivalent to loss due to sample removal. This indicates that rates of net H_2 oxidation exceeding those measured in abiotic controls can be ascribed to biological activity.

All microcosms exhibited an initial lag phase, defined as the time between introduction of the substrate (H_2) and its detectable consumption by microbial activity (Fig. 1 *A* and *C*). In KJ microcosms, the lag phase lasted no more than 12 d. In contrast, the lag phase for RG sediments lasted 18 d under most conditions. While RG sediments were frozen in storage for several years between their collection in 2009 and their use as inocula here, the lag times observed in this experiment match closely with those observed in other growth experiments that used RG sediments stored for between 1 and 5 y (8, 23, 47). Indeed, similar lag times were associated with the onset of CO_2 fixation using the same sediments collected from RG in 2009 but frozen for 2 y (8) versus 9 y in the present study. This suggests that any deleterious effects of long-term storage on RG sediment microbiota were minimal.

It has been suggested that the duration of the lag phase can be used as a proxy for the degree of adaptation by a given microorganism (or community of microorganisms) to use a given substrate (55, 56), with shorter lag times indicative of a greater degree of adaptation. In this context, the results of the current study suggest that hydrogenotrophic members of the microbial communities inhabiting KJ sediments may be better adapted to take advantage of H_2 as an electron donor than those of RG sediments. Alternatively, hydrogenotrophs may be numerically more abundant at KJ than RG.

The most straightforward approach to addressing the likelihood of these possibilities would be to use molecular methods to determine the abundance of organisms with the genomic capacity to oxidize H_2. However, numerous attempts to extract genomic DNA from KJ sediments, including using methods specifically developed for basaltic sediments (57), failed to yield detectable (>0.5 ng DNA per gdws) DNA. Moreover, extracts did not yield PCR amplicons when probed using universal 16S rRNA gene primers. This prevented application of molecular approaches to characterize endogenous sediment communities in KJ and to estimate their abundance.

To further examine the role of H_2 oxidation in supporting subglacial and proglacial sediment communities, the maximum rate of net H_2 oxidation was determined. This rate ranged from 2.9 to 9.3 (median, 7.6) nmol·d^{-1}·$gdws^{-1}$ for KJ microcosms and from 0.8 to 2.3 (median, 1.1) nmol·d^{-1}·$gdws^{-1}$ for RG microcosms (Fig. 2 and *SI Appendix*, Table S3). Maximum rates of net H_2 oxidation in KJ microcosms were up to 10-fold higher than those in RG microcosms, adding further support to the hypothesis that the microbial communities associated with KJ sediments are better adapted to use H_2 as a reductant. For perspective, maximum net rates of H_2 oxidation in KJ were within an order of magnitude of those (~84 nmol H_2·d^{-1}·$gdws^{-1}$) measured in Antarctic desert surface soils incubated at a slightly higher temperature [10 °C (58)].

Rates of Net CO_2 Fixation. A second set of microcosm assays was conducted to measure rates of net CO_2 fixation among members of the KJ and RG sediment communities and to gauge whether autotrophy is coupled to hydrogenotrophy in either community, in addition to the extent to which this is similarly (or not) influenced by oxidant amendment. Each microcosm contained H_2 and CO_2 (a fraction labeled as $^{14}CO_2$) and was amended with O_2, NO_3^-, hematite, SO_4^{2-}, or was unamended (CO_2 only) (Fig. 1 *B* and *D*). No microcosms were amended with ferrihydrite because, in H_2 oxidation assays, there was no discernable difference in activity between microcosms amended with ferrihydrite and those amended with hematite.

In heat-killed control microcosms containing sediments from KJ and RG, net uptake of $^{14}CO_2$ did not occur (Fig. 1 *B* and *D*). In contrast, net uptake of $^{14}CO_2$ began to increase after an initial lag phase in all test microcosms. In KJ microcosms, the lag phase lasted 7 to 14 d, depending on the supplied oxidant, whereas in RG microcosms it lasted ~28 d regardless of oxidant. The lengths

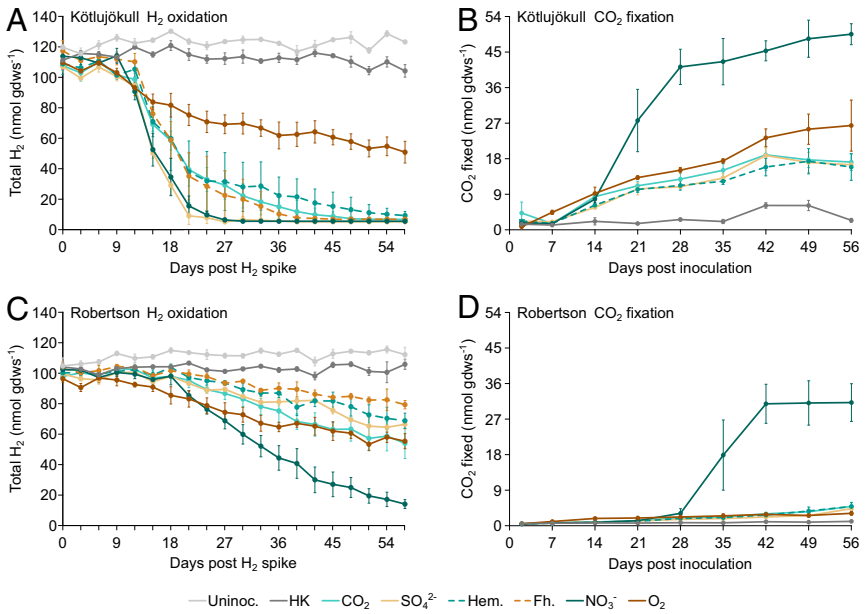

Fig. 1. H_2 content (*A* and *C*) and carbon fixation (*B* and *D*) in microcosms inoculated with proglacial or subglacial sediments from KJ (*A* and *B*) or RG (*C* and *D*), respectively, and incubated in the dark at 4 °C. The means and SDs of measurements from triplicate microcosms are presented. Abbreviations: Fh., ferrihydrite; gdws, gram dry weight sediment; Hem., hematite; HK, heat-killed control; Uninoc., uninoculated control.

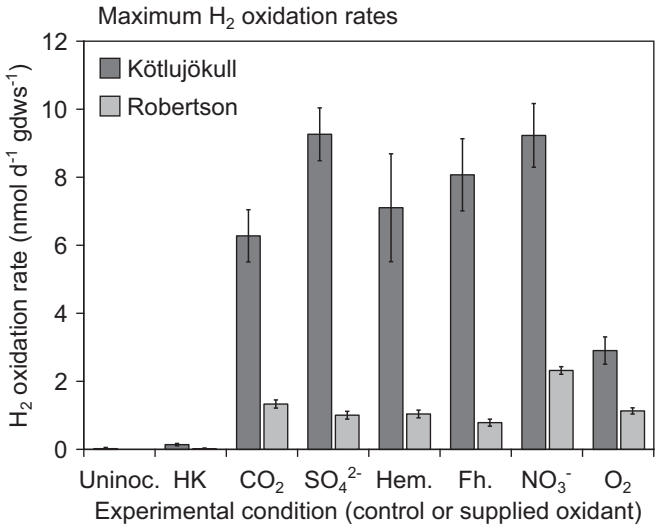

Fig. 2. Maximum H_2 oxidation rates in microcosms containing proglacial or subglacial sediments from KJ or RG, respectively, when incubated in the dark at 4 °C. Linear regressions were applied to selected data from the sets represented in Fig. 1 *A* and *C*, and the inverse of the slope of each regression is reported. Error bars represent the SD associated with the slope of each regression. Abbreviations: Fh., ferrihydrite; gdws, gram dry weight sediment; Hem., hematite; HK, heat-killed control; Uninoc., uninoculated control.

of these lag phases match closely with those measured for net H_2 oxidation in KJ microcosms, while they are roughly 1.5 times longer than those measured for net H_2 oxidation in RG microcosms. This suggests that H_2 may be the primary reductant supporting CO_2 fixation for at least part of the KJ community, while its primary role in RG may be to supplement facultatively autotrophic or mixotrophic (with respect to electron donor) microbial populations. Support for this possibility comes from the relatively high levels of TOC in RG subglacial sediments (24.8 ± 14.0 mg·$gdws^{-1}$; Table 1) and their porewaters [~60 μM (47)], a characteristic that would otherwise be expected to promote chemoheterotrophy or chemolithoheterotrophy over chemolithoautotrophy, as has been shown for other natural systems (59) and cultures (60, 61). In contrast, the amount of TOC in KJ sediments is below the practical limit of quantitation for the instrumentation and techniques used in this study (<1.06 mg·$gdws^{-1}$). Extrapolation beyond the lower quantitation limit based on the slope of the calibration curve indicates that TOC in KJ sediments is roughly two orders of magnitude lower than in RG sediments (0.38 ± 0.14 mg $gdws^{-1}$; Table 1).

The maximum rate of net CO_2 fixation ranged from 0.37 to 2.39 (median, 0.44) nmol C·d^{-1}·$gdws^{-1}$ for KJ and from 0.04 to 1.98 (median, 0.08) nmol C·d^{-1}·$gdws^{-1}$ for RG microcosms (Fig. 3 and *SI Appendix*, Table S6). Rates of net CO_2 fixation were 4.8- to 12.2-fold higher in KJ microcosms than in RG microcosms for oxidants other than NO_3^-. The dramatic increase in both maximum CO_2 fixation rate and total accumulated fixed CO_2 in microcosms amended with NO_3^- is a notable feature of each dataset, and is consistent with previous evidence indicating the potential for NO_3^- reduction in subglacial environments from a variety of catchments (62, 63), including those from RG (47). For comparison, a previous measurement of the rate of CO_2 fixation (1.2 ± 0.7 nmol C·d^{-1}·$gdws^{-1}$) in unamended (no added H_2 or exogenous oxidant) microcosm assays containing RG sediments incubated over a period of 176 d (8) falls between the low rates described above and that observed in RG microcosms amended with NO_3^-, which was 1.98 ± 0.39 nmol C·d^{-1}·$gdws^{-1}$.

Given the extremely low nitrogen content of sediments from both catchments (KJ, <27 μg·$gdws^{-1}$; RG, 212.7 ± 54.2 μg·$gdws^{-1}$; Table 1) and their correspondingly high organic C:N ratios, it is possible that the addition of NO_3^- simply relieved fixed N limitation, thereby increasing the metabolic activities of all members of these communities. However, given that in RG microcosm assays H_2 oxidation commenced prior to CO_2 fixation, it is unlikely the two processes are tightly linked in the metabolism of a single microbial population. In any case, the higher rates of both H_2 oxidation and CO_2 fixation in KJ microcosms, and their matching lag times, together point to the linking of these processes in KJ sediments much more strongly than in RG sediments.

KJ and RG microcosms amended with ferrihydrite and hematite, as well as RG microcosms amended with SO_4^{2-}, exhibited maximum rates of net H_2 oxidation and CO_2 fixation that were similar to unamended (CO_2 only) controls (Figs. 2 and 3). This suggests that dominant primary producers are either 1) using CO_2 as an oxidant (i.e., they are acetogens or methanogens) or 2) utilizing an oxidant or reductant endogenous to their source sediments in lieu of those supplied experimentally. Microcosms were therefore probed for evidence of these two possibilities. Neither acetate nor CH_4 were detected in the medium or headspace of any of the microcosm assays. Similarly, no microcosm medium contained dissolved sulfide, even when SO_4^{2-} had been added. Ferrous iron was detected in microcosms amended with ferrihydrite (KJ, mean ± SD, 22.7 ± 9.0 μM; RG, 74.8 ± 62.3 μM), hematite (KJ, 40.7 ± 7.6 μM; RG, 20.3 ± 5.1 μM), SO_4^{2-} (KJ, 33.2 ± 5.4 μM; RG, 39.5 ± 27.9 μM), and CO_2 only (KJ, 20.9 ± 2.9 μM; RG, 8.7 ± 4.4 μM), but was also present in KJ heat-killed control microcosms (13.2 ± 0.9 μM), which might be expected given the Fe(II) content of the iron rich basaltic sediments at KJ. NO_2^-, an intermediate in the reduction of NO_3^-, was present in NO_3^--amended microcosms from both catchments (KJ, 131.4 ± 8.5 μM; RG, 5.8 ± 2.7 μM), suggesting that NO_3^- may stimulate both hydrogen oxidation and CO_2 fixation in both systems.

Abundance of Hydrogenotrophs and Oxidant Coupling. To further investigate the abundance of hydrogenotrophs and the oxidants that couple with H_2 oxidation in KJ and RG sediment populations, an MPN cultivation approach was undertaken (Fig. 4). Microcosm

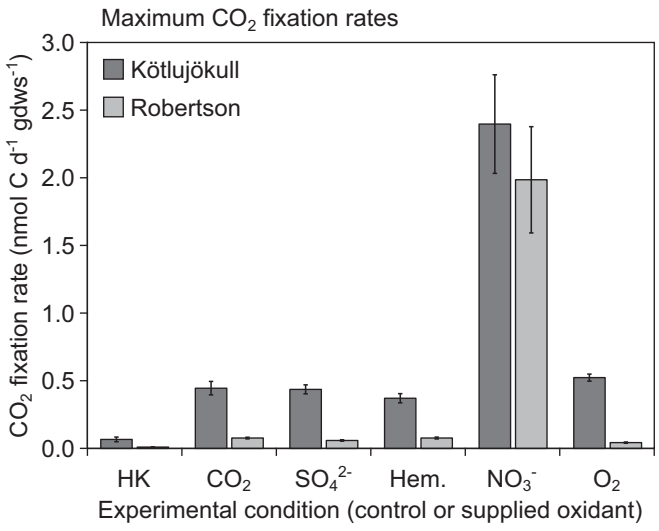

Fig. 3. Maximum CO_2 fixation rates within microcosms containing proglacial or subglacial sediments from KJ or RG, respectively, when incubated in the dark at 4 °C. Linear regressions were applied to selected data from the sets represented in Fig. 1 *B* and *D*, and the slope of each regression is reported. Error bars represent the SD associated with the slope of each regression. Abbreviations: gdws, gram dry weight sediment; Hem., hematite; HK, heat-killed control. Microcosms were not amended with ferrihydrite for this experiment given the similar rates of H_2 oxidation in ferrihydrite- and hematite-amended microcosms.

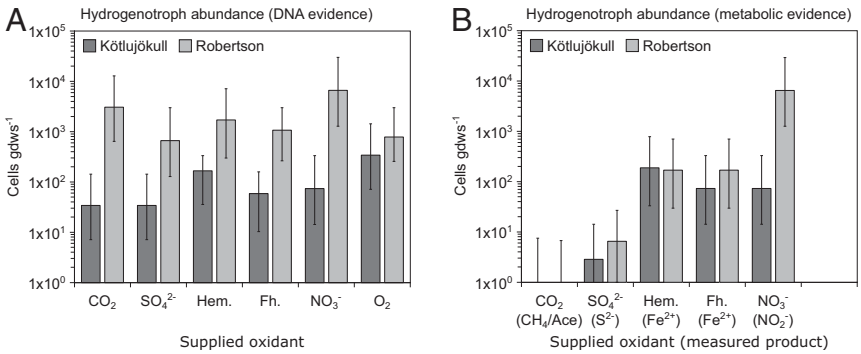

Fig. 4. Abundance of hydrogenotrophic cells capable of autotrophic growth as determined by most probable number (MPN) assays containing dilutions of proglacial or subglacial sediments from KJ or RG, respectively. The MPN was assessed first by quantifying total extractable DNA (*A*) and further refined by measurement of the metabolic products of CO_2, SO_4^{2-}, Fe(III), or NO_3^- reduction (methane and/or acetate, sulfide, ferrous iron, and nitrite, respectively) (*B*). Microbial growth was detected in CO_2- and SO_4^{2-}-amended microcosms without associated reduction of CO_2 or SO_4^{2-}. This observation led to the hypothesis that growth under these conditions is supported by heterotrophy. Error bars represent 95% confidence intervals. Abbreviations: Ace., acetate; Fh., ferrihydrite; gdws, gram dry weight sediment; Hem., hematite.

assays containing M9 minimal medium, with H_2 as the sole added reductant and CO_2 as the sole added carbon source, were amended with O_2, NO_3^-, ferrihydrite, hematite, SO_4^{2-}, or were not amended (CO_2 only). Surprisingly, there were between 2- and 90-fold more cultivatable hydrogenotrophs in RG sediments than in those from KJ. This observation is consistent with the higher amounts of DNA recovered from RG sediments (7.4 ng·gdws^{-1}) when compared to KJ sediments (<0.5 ng·gdws^{-1}). To the extent that cultivation and DNA extraction/recovery bias was minimized in these experiments, these data suggest that the faster onset and higher rates of microbial H_2 oxidation and CO_2 fixation activity observed in KJ sediment microcosms described above are unlikely to result from a greater in situ abundance of hydrogenotrophic cells. Rather, they suggest that the community inhabiting KJ sediments is assembled to include populations better adapted to efficiently utilize available nutrients such as H_2, which is at a concentration in KJ meltwaters that is nearly an order of magnitude greater than observed in RG meltwaters.

A related possibility is that the apparent abundance of hydrogenotrophs at RG reflects populations that are mixotrophic and/or can facultatively oxidize H_2. Evidence in support of this possibility comes from physiological and genomic studies of the dominant primary producer in RG sediments, *Thiobacillus* sp. RG5 (8). This strain is supported primarily by products (e.g., thiosulfate) of abiotic FeS_2 oxidation, but its genome also encodes a group 1 [NiFe]-hydrogenase (7) that is predicted to function in H_2 oxidation (20). While growth experiments aimed at evaluating H_2 transformation were not conducted with *Thiobacillus* sp. RG5, they have been conducted with a close relative, *Thiobacillus denitrifications*. *T. denitrificans* also encodes a group 1 [NiFe]-hydrogenase but was shown to be unable to use H_2 as sole electron donor when growing autotrophically via NO_3^- reduction (64). This suggests the possibility for mixotrophic energy metabolism as it relates to H_2, as has been shown for other organisms (60, 61).

MPNs were evaluated by quantifying DNA and reduced products from supplied oxidants. When MPNs were estimated using total extractable DNA, the abundance of hydrogenotrophs in both KJ and RG sediments differed by less than an order of magnitude among experimental conditions (supplied oxidants) (Fig. 4*A*). KJ sediment MPNs estimated by total extractable DNA were not substantially different from those estimated by the detection of Fe^{2+} for ferrihydrite- and hematite-amended microcosms, nor were DNA-based MPN estimates different from those based on detection of NO_2^- for NO_3^--amended KJ and RG microcosms (Fig. 4*B*). However, MPNs estimated based on the detection of products of the reduction of SO_4^{2-} and CO_2 did substantially differ from those based on total extractable DNA (Fig. 4 *A* and *B*). Given that sediments from both RG and KJ are known to contain iron oxides (*SI Appendix*, Fig. S1) (65, 66), it is possible that sulfide generated from SO_4^{2-} reduction was oxidized by Fe(III) in a cryptic cycle similar to what has been described for other freshwater sediment ecosystems (67). However, the similar numbers of hydrogenotrophs in the SO_4^{2-} (also containing CO_2) and CO_2-only conditions, combined with the absence of detectable methane or acetate in MPN and microcosm assays, indicate instead that the microbial populations enriched under the CO_2-only and SO_4^{2-}-amended conditions (for both KJ and RG sediments) likely possess mixotrophic metabolisms in which H_2 oxidation is not necessarily coupled to autotrophy. As such, these cells may have been supported by remnant organic carbon in sediments used to inoculate the MPN enrichment series.

The observation of similar MPN estimates derived from DNA extraction and Fe^{2+} detection in hematite- and ferrihydrite-amended KJ sediments (Fig. 4), combined with evidence for both net H_2 oxidation and CO_2 fixation in hematite- and ferrihydrite-amended KJ microcosms (Figs. 1–3), point to potential coupling of H_2 oxidation, iron reduction, and CO_2 fixation in KJ sediments. To further investigate this possibility, microcosms containing M9 minimal growth medium amended with H_2, CO_2, and hematite were inoculated with MPN cultures exhibiting both microbial growth and iron reduction. Due to the dilution of glacial sediment during preparation of MPN cultures and their subsequent transfer into M9 medium, the transfer of endogenous oxidants and organic carbon to these cultures was presumed to be negligible [transfer cultures estimated to contain 0.6 μg TOC·mL^{-1} after ~600-fold (vol/vol) dilution of sediments]. Continued growth of a single morphotype was observed, and this growth was associated with the production of Fe^{2+} (Fig. 5). Given that CO_2 was the only provided carbon source and H_2 the only provided reductant, these observations point to this population coupling H_2 oxidation with the reduction of hematite to fuel autotrophic growth. While H_2 oxidizing, chemolithoautotrophic Fe(III) reducers are known to occur in high-temperature environments (68, 69) and have recently been identified in low-pH, moderate-temperature environments (70), to our knowledge such organisms have not previously been identified in low-temperature environments of circumneutral pH.

MPN (Meta)genomic Sequence Analysis. Nutrient amendments that promoted both H_2 oxidation and CO_2 fixation were targeted to identify the population(s) responsible for the observed activities and to probe mechanisms of H_2 oxidation in these taxa. These amendments included NO_3^-, hematite, ferrihydrite, SO_4^{2-}, and

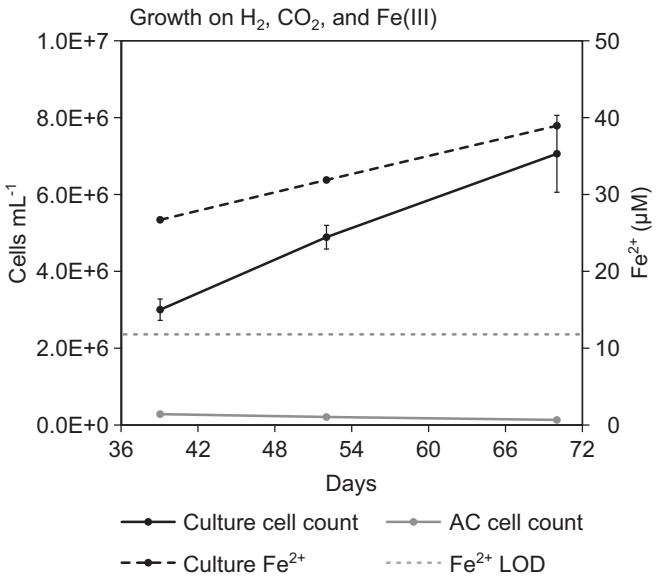

Fig. 5. Activity and growth of a KJ most probable number (MPN) culture amended with H_2, CO_2, and hematite when transferred into fresh medium containing these components. (Meta)genomic sequencing of DNA extracted from this culture reveals a single metagenome assembled genome affiliated (94% RpoB ID) with *Rhodoferax ferrireducens*. Culture Fe^{2+} content was calculated as the concentration of Fe^{2+} measured in the experimental microcosm minus that measured in the abiotic control. Error bars represent SEM. Abbreviations: AC, abiotic control; LOD, limit of detection.

CO_2 alone for KJ sediments and NO_3^- for RG sediments. MPN cultures grown with each of these amendments were subjected to DNA extraction and metagenomic sequencing. The composition of each sequenced MPN community is shown in Table 2, while the completeness and contamination of each recovered metagenome assembled genome (MAG) is presented in *SI Appendix*, Table S7.

Sequencing of genomic DNA from KJ MPN assays amended with H_2/CO_2 only and with $H_2/CO_2/SO_4^{2-}$ yielded the same three MAGs. The most abundant MAG in the H_2/CO_2-only and the $H_2/CO_2/SO_4^{2-}$-amended MPNs (93% and 89% of total reads, respectively) exhibited close affiliation (92% identity at the amino acid level of the RNA polymerase β-subunit [RpoB] for both bins) with *Glaciimonas*, a metabolically flexible genus common to glacial ecosystems (e.g., refs. 71–73). Both *Glaciimonas* MAGs encode homologs of [NiFe]-hydrogenases and ribulose-1,5-bisphosphate carboxylase/oxygenase (RuBisCO), consistent with an ability to grow autotrophically using H_2 as an electron donor. However, despite being 99% similar at the level of RpoB sequence identity, the two MAGs differed in the complements of encoded [NiFe]-hydrogenases. Both *Glaciimonas* MAGs encode homologs of group 2b H_2 sensing [NiFe]-hydrogenases that regulate transcription and maturation of oxidative [NiFe]-hydrogenases (20, 74). In addition to the group 2b homolog, the *Glaciimonas* MAG from the $H_2/CO_2/SO_4^{2-}$-amended microcosm encodes a group 1d oxidative [NiFe]-hydrogenase and the MAG from the H_2/CO_2-amended microcosm encodes a bidirectional group 3d [NiFe]-hydrogenase. The presence of both an H_2 sensing and an oxidative [NiFe]-hydrogenase points to adaptation to efficiently utilize H_2 when it is available while potentially minimizing costs associated with de novo protein and cofactor biosynthesis. However, the presence of a bidirectional hydrogenase in the H_2/CO_2 *Glaciimonas* MAG, rather than an oxidative hydrogenase as found in the $H_2/CO_2/SO_4^{2-}$ MAG, casts doubt on the reliance of this population on H_2 as its sole source of electrons during growth and could be further evidence of mixotrophic or facultatively autotrophic metabolism. Homologs of the dissimilatory bisulfite reductase, a gene required for reduction of SO_4^{2-}, were not detected in either *Glaciimonas* MAG, consistent with the absence of detectable sulfide in KJ MPN and activity assay microcosms amended with SO_4^{2-}.

Sequencing of DNA extracted from hematite- and ferrihydrite-amended KJ MPNs failed. However, a single transfer of the H_2/CO_2/hematite-amended MPN into fresh medium grew (Fig. 5), and this culture was subjected to DNA extraction and (meta)genomic sequencing. Both the hematite KJ MPN transfer culture and NO_3^--amended KJ MPN culture comprised a dominant MAG that was closely related (94% RpoB sequence identity) to *Rhodoferax ferrireducens*, a genus that is commonly identified in subglacial habitats (62, 75) including RG (3, 6). Interestingly, like one of the *Glaciimonas* MAGs, the *Rhodoferax* MAG encoded homologs of a group 2b H_2 sensing [NiFe]-hydrogenase and a group 1d uptake [NiFe] hydrogenase, again pointing to adaptation to effectively respond to H_2 availability and use it as a component of energy metabolism. The MAG also encoded RuBisCO and dissimilatory nitrate reductase (NarGHJI), consistent with the stimulation of H_2 oxidation and CO_2 fixation by amendment with NO_3^-. Importantly, *Rhodoferax ferrireducens* strains have been shown to be metabolically flexible, displaying growth phenotypes as diverse as photoheterotrophy, aerobic heterotrophy, and fermentation (76). To our knowledge, however, H_2-dependent chemolithoautotrophic growth has not so far been observed in this genus.

Despite evidence for iron reduction in KJ MPN assays, activity assays, and transfer cultures containing *Rhodoferax*, we were unable to identify genes encoding the porin cytochrome complexes that have been implicated in Fe(III) reduction in other bacteria. Notably, both the Pcc system used by *Geobacter* and several other metal-reducing organisms (77, 78) and the Mtr system that plays a similar role in *Shewanella* (79, 80) were absent from the *Rhodoferax* MAGs, despite each being estimated to be 99% complete. Shi et al. (79) previously reported the discovery of homologs of MtrABC and accessory proteins encoded in the genome of *R. ferrireducens* using a BLAST-based approach. However, a BLASTp analysis of amino acid sequences of MtrABC in *Shewanella oneidensis* against the genome of *R. ferrireducens* only revealed a homolog of the MtrA subunit (*e* value <1E-70). No homologs of MtrABC were detected in the KJ-derived *Rhodoferax* MAGs. Importantly, dissimilatory iron reduction has been demonstrated in *R. ferrireducens* (81) despite this lack of evidence for the presence of known Fe(III) reduction pathways in its genome or in the KJ-derived *Rhodoferax* MAGs.

The only nutrient that stimulated both net H_2 oxidation and CO_2 fixation at RG was NO_3^- (Fig. 1 *C* and *D*). For this reason, only the NO_3^--amended RG MPN was subjected to metagenomic sequencing and analysis. Two MAGs were identified in this MPN and were both affiliated with *Polaromonas* strains. While both MAGs encoded homologs of RuBisCO and dissimilatory nitrate reductase (NarGHJI), neither encoded homologs of [FeFe]- or [NiFe]-hydrogenases or proteins involved in their maturation. Thus, it is not clear how these organisms were growing in MPN assays unless they were using an endogenous reductant, such as organic carbon, FeS_2, or products derived from FeS_2 oxidation. Importantly, a transfer of this MPN into the same medium did not yield growth, consistent with the use of an endogenous reductant in the MPN assays.

Conclusions

Both silicate- and iron-bearing minerals can generate H_2 through cataclastic radical and reductive mechanisms in the presence of water. These minerals are chemically altered in the process, however, thereby preventing sustained reactivity unless they are resurfaced. Glacial comminution is one mechanism of generating fresh mineral surfaces capable of reacting with water on a continual basis. Thus, subglacial environments have the potential to provide continuous

Table 2. Composition of communities from the most dilute MPN assays amended with H_2, CO_2, and (where indicated) other oxidants and containing proglacial or subglacial sediments from Kötlujökull or Robertson Glacier, respectively

Glacier	Supplied oxidant	% Binned populations	Taxon	RpoB identity	Hydrogenase (subgroup)	CO_2 fixation marker	Terminal reductase
Kötlujökull	CO_2	92.9	*Glaciimonas* sp. PCH181	91.9%	HupUV (2b), HoxYH (3d)	CbbSL	
		3.9	*Cellulomonas* sp. WB94	99.2%	HydA (A1)	None	
		3.3	*Phycicoccus* sp. Soil748	93.5%	HyhBGSL (3b)	None	
	SO_4^{2-}	88.5	*Glaciimonas* sp. PCH181	92.0%	HupUV (2b), HyaABC (1d)	CbbSL	
		3.5	*Phycicoccus* sp. Soil748	93.8%	HyhBGSL (3b)	None	
		4.3	*Cellulomonas* sp. WB94	99.2%	HydA (A1)	None	
	Hem.*	97.3	*Rhodoferax ferrireducens*	93.7%	HupUV (2b), HyaABC (1d)	CbbM	NarGHJI
		2.7	*Polaromonas* sp. CF318	95.6%	HupUV (2b)	None	NarGHJI
	NO_3^-	100.0	*Rhodoferax ferrireducens*	93.7%	HupUV (2b), HyaABC (1d)	CbbM	NarGHJI
Robertson	NO_3^-	96.7	*Polaromonas* sp. A23	96.9%	None	CbbSL	NarGHJI
		3.3	*Polaromonas glacialis*	98.1%	None	4-Hydroxybutyryl-CoA dehydratase	NarGHJI

Community DNA was extracted and subjected to metagenomic sequencing to reveal the relative abundance of metagenome assembled genomes (MAGs) in the community, the taxonomic composition of MAGs via RNA polymerase β-subunit (RpoB) homology, and the presence of protein homologs that would allow for H_2 oxidation, CO_2 fixation, and the coupling of H_2 oxidation with supplied oxidants. Abbreviations: CbbM, the large subunit of the proteobacterial form II (L_2) ribulose-1,5-bisphosphate carboxylase/oxygenase; CbbSL, the small and large subunits of ribulose-1,5-bisphosphate carboxylase/oxygenase involved in the Calvin cycle, respectively; Hem., hematite; HoxYH, the small and large subunits of the group 3d bidirectional [NiFe]-hydrogenase (20); HupUV, the small and large subunits of the group 2b sensory [NiFe]-hydrogenase; HyaABC, the small, large, and cytochrome subunits of the group 1d uptake [NiFe]-hydrogenase, respectively; HydA, the catalytic subunit of [FeFe]-hydrogenases; HyhBGSL, the iron–sulfur, diaphorase, small, and large subunits of the group 3b bidirectional [NiFe]-hydrogenase, respectively; NarGHJI, the α, β, molybdenum cofactor assembly chaperone, and γ subunits of the dissimilatory nitrate reductase complex, respectively.

*The MAGs described for Kötlujökull hematite-amended MPN assays were recovered from a culture transferred into fresh medium, the growth and Fe(III) reduction activity of which are depicted in Fig. 5.

sources of chemical energy, in the form of disequilibrium between H_2 and oxidized minerals, that can support chemolithotrophic microbial primary production in subglacial and downstream proglacial environments.

Meltwaters from KJ, which overlays a basaltic catchment, had an order of magnitude more dissolved H_2 than those from RG, which sits in a carbonate catchment. The sediment community at KJ exhibited shorter lag times and significantly faster rates of H_2 oxidation and CO_2 fixation than those measured for the RG sediment community. Metabolic activity assays and MPN experiments show that at least two populations of autotrophic hydrogenotrophs inhabit KJ sediments: one metabolically flexible mixotroph (*Glaciimonas* sp.) and one that can, at a minimum, utilize H_2, CO_2, and Fe(III) or NO_3^- (*Rhodoferax* sp.). In RG sediments, however, differing lag times between H_2 oxidation and CO_2 fixation experiments suggest that the two processes are not tightly coupled. A potential explanation for this comes from a prior study that showed the dominant primary producer in RG sediments depended primarily on FeS_2 or derivatives of its oxidation (i.e., thiosulfate) as reductants (7, 8). Thus, H_2 oxidation in RG sediment populations may be attributable to a mixotrophic or chemolithoheterotrophic metabolism, as has been recently demonstrated in other taxa (60, 61).

(Meta)genomic sequencing of the most dilute MPN assays from KJ identified a relative of the NO_3^-- and Fe(III)-reducing *Rhodoferax* and a population of *Glaciimonas* as the dominant H_2 oxidizing autotrophs and/or mixotrophs in this system. Transfers of the *Rhodoferax* MPN culture into fresh medium further demonstrated the ability of this population to grow autotrophically using the H_2/Fe(III) redox couple. This represents the only report to date of chemolithoautotrophic, H_2-dependent iron reduction in a nonhyperthermophilic or acidophilic organism, and experiments to further characterize this bacterium are underway.

Collectively, these results indicate that differences in bedrock mineral composition likely influence supplies of lithogenic H_2 and oxidants and that these, in turn, influence the diversity, abundance, and activity of H_2-dependent autotrophs in subglacial and proglacial habitats. More broadly, they further underscore the importance of physical and chemical weathering processes in releasing nutrients capable of sustaining microbial primary production in these habitats, corroborating recent evidence that such communities could be supported by chemolithotrophic primary production, independent of photosynthetically fixed carbon (8). This finding has important implications for the survival of terrestrial life through Snowball Earth periods of globally extensive glaciation (82, 83) and for the possibility of discovering life on other icy planetary bodies (84). Indeed, the recent discovery of H_2 gas in plumes of material erupting from the icy crust of Enceladus (85) points to active rock–water interactions occurring beneath the ice surface and implies a subsurface geochemical system with potentially important parallels to that of KJ and other glaciers in basaltic terrains.

Data Availability. Metagenomic sequence data have been deposited in the NCBI BioProject database (ID no. PRJNA622799).

ACKNOWLEDGMENTS. This work was supported by a grant (NNX16AJ64G) from the National Aeronautics and Space Administration Exobiology and Evolutionary Biology program to M.L.S. and E.S.B. E.C.D. was supported by an NSF Graduate Research Fellowship.

1. M. L. Skidmore, J. M. Foght, M. J. Sharp, Microbial life beneath a high Arctic glacier. *Appl. Environ. Microbiol.* **66**, 3214–3220 (2000).
2. M. Sharp *et al*., Widespread bacterial populations at glacier beds and their relationship to rock weathering and carbon cycling. *Geology* **27**, 107–110 (1999).
3. T. L. Hamilton, J. W. Peters, M. L. Skidmore, E. S. Boyd, Molecular evidence for an active endogenous microbiome beneath glacial ice. *ISME J.* **7**, 1402–1412 (2013).
4. K. A. Cameron *et al*., Meltwater export of prokaryotic cells from the Greenland ice sheet. *Environ. Microbiol.* **19**, 524–534 (2017).
5. R. S. Hindshaw, T. H. E. Heaton, E. S. Boyd, M. R. Lindsay, E. T. Tipper, Influence of glaciation on mechanisms of mineral weathering in two high Arctic catchments. *Chem. Geol.* **420**, 37–50 (2016).
6. A. C. Mitchell, M. J. Lafrenière, M. L. Skidmore, E. S. Boyd, Influence of bedrock mineral composition on microbial diversity in a subglacial environment. *Geology* **41**, 855–858 (2013).
7. Z. R. Harrold *et al*., Aerobic and anaerobic thiosulfate oxidation by a cold-adapted, subglacial chemoautotroph. *Appl. Environ. Microbiol.* **82**, 1486–1495 (2015).
8. E. S. Boyd, T. L. Hamilton, J. R. Havig, M. L. Skidmore, E. L. Shock, Chemolithotrophic primary production in a subglacial ecosystem. *Appl. Environ. Microbiol.* **80**, 6146–6153 (2014).
9. S. N. Montross, M. Skidmore, M. Tranter, A. L. Kivimaki, R. J. Parkes, A microbial driver of chemical weathering in glaciated systems. *Geology* **41**, 215–218 (2013).
10. H.-W. Hsu *et al*., Ongoing hydrothermal activities within Enceladus. *Nature* **519**, 207–210 (2015).
11. J. R. Spear, J. J. Walker, T. M. McCollom, N. R. Pace, Hydrogen and bioenergetics in the Yellowstone geothermal ecosystem. *Proc. Natl. Acad. Sci. U.S.A.* **102**, 2555–2560 (2005).
12. M. R. Lindsay *et al*., Probing the geological source and biological fate of hydrogen in Yellowstone hot springs. *Environ. Microbiol.* **21**, 3816–3830 (2019).
13. L.-H. Lin *et al*., Radiolytic H_2 in continental crust: Nuclear power for deep subsurface microbial communities. *Geochem. Geophys. Geosyst.* **6**, (2005).
14. K. H. Nealson, F. Inagaki, K. Takai, Hydrogen-driven subsurface lithoautotrophic microbial ecosystems (SLiMEs): Do they exist and why should we care? *Trends Microbiol.* **13**, 405–410 (2005).
15. J. Telling *et al*., Rock comminution as a source of hydrogen for subglacial ecosystems. *Nat. Geosci.* **8**, 851–854 (2015).
16. M. L. Macdonald, J. L. Wadham, J. Telling, M. L. Skidmore, Glacial erosion liberates lithologic energy sources for microbes and acidity for chemical weathering beneath glaciers and ice sheets. *Front. Earth Sci.* **6**, 212 (2018).
17. D. S. Kelley *et al*., A serpentinite-hosted ecosystem: The lost city hydrothermal field. *Science* **307**, 1428–1434 (2005).
18. T. O. Stevens, J. P. McKinley, Abiotic controls on H_2 production from basalt-water reactions and implications for aquifer biogeochemistry. *Environ. Sci. Technol.* **34**, 826–831 (2000).
19. E. S. Boyd, T. L. Hamilton, J. R. Spear, M. Lavin, J. W. Peters, [FeFe]-hydrogenase in Yellowstone National Park: Evidence for dispersal limitation and phylogenetic niche conservatism. *ISME J.* **4**, 1485–1495 (2010).
20. J. W. Peters *et al*., [FeFe]- and [NiFe]-hydrogenase diversity, mechanism, and maturation. *Biochim. Biophys. Acta* **1853**, 1350–1369 (2015).
21. I. Kita, S. Matsuo, H. Wakita, H_2 generation by reaction between H_2O and crushed rock: An experimental study on H_2 degassing from the active fault zone. *J. Geophys. Res. Solid Earth* **87**, 10789–10795 (1982).
22. R. J. Parkes *et al*., Rock-crushing derived hydrogen directly supports a methanogenic community: Significance for the deep biosphere. *Environ. Microbiol. Rep.* **11**, 165–172 (2019).
23. E. S. Boyd, M. Skidmore, A. C. Mitchell, C. Bakermans, J. W. Peters, Methanogenesis in subglacial sediments. *Environ. Microbiol. Rep.* **2**, 685–692 (2010).
24. A. B. Michaud *et al*., Microbial oxidation as a methane sink beneath the West Antarctic Ice Sheet. *Nat. Geosci.* **10**, 582–586 (2017).
25. H. Ma *et al*., *Ex situ* culturing experiments revealed psychrophilic hydrogentrophic methanogenesis being the potential dominant methane-producing pathway in subglacial sediment in Larsemann Hills, Antarctic. *Front. Microbiol.* **9**, 237 (2018).
26. Z. Yang *et al*., H_2 metabolism revealed by metagenomic analysis of subglacial sediment from East Antarctica. *J. Microbiol.* **57**, 1095–1104 (2019).
27. A. Gale, C. A. Dalton, C. H. Langmuir, Y. Su, J.-G. Schilling, The mean composition of ocean ridge basalts. *Geochem. Geophys. Geosyst.* **14**, 489–518 (2013).
28. J. Kruger, Development of minor outwash fans at Kötlujökull, Iceland. *Quat. Sci. Rev.* **16**, 649–659 (1997).
29. H. Jóhannesson, *Geological Map of Iceland. Bedrock Geology* (Icelandic Institute of Natural History, Reykjavík, 2014).
30. C. Lacasse *et al*., Bimodal volcanism at the Katla subglacial caldera, Iceland: Insight into the geochemistry and petrogenesis of rhyolitic magmas. *Bull. Volcanol.* **69**, 373 (2006).
31. M. E. McMechan, *Geology, Peter Lougheed Provincial Park, Rocky Mountain Front Ranges* (Geological Survey of Canada, Ottawa, ON, Canada, 1989).
32. M. Sharp, R. A. Creaser, M. Skidmore, Strontium isotope composition of runoff from a glaciated carbonate terrain. *Geochim. Cosmochim. Acta* **66**, 595–614 (2002).
33. R. K. Griggs, "Characterization of subglaical till from Robertson Glacier, Alberta, Canada: Implications for biogeochemical weathering," MS thesis, Department of Earth Sciences, Montana State University, Bozeman, MT (2013).
34. J. K. Fogo, M. Popowsky, Spectrophotometric determination of hydrogen sulfide—methylene blue method. *Anal. Chem. (Wash.)* **21**, 732–734 (1949).
35. F. H. Chapelle, D. A. Vroblesky, J. C. Woodward, D. R. Lovley, Practical considerations for measuring hydrogen concentrations in groundwater. *Environ. Sci. Technol.* **31**, 2873–2877 (1997).
36. M. R. Lindsay *et al*., Subsurface processes influence oxidant availability and chemoautotrophic hydrogen metabolism in Yellowstone hot springs. *Geobiology* **16**, 674–692 (2018).
37. R. M. Atlas, *Handbook of Microbiological Media* (ASM Press, Washington, DC, 2004).
38. K. L. Straub, A. Kappler, B. Schink, Enrichment and isolation of ferric-iron- and humic-acid-reducing bacteria. *Methods Enzymol.* **397**, 58–77 (2005).
39. K. R. Mitchell, C. D. Takacs-Vesbach, A comparison of methods for total community DNA preservation and extraction from various thermal environments. *J. Ind. Microbiol. Biotechnol.* **35**, 1139–1147 (2008).
40. R. Blodgett, "Appendix 2: Most probable number from serial dilutions" in *Bacteriological Analytical Manual* (US Food and Drug Administration, 2010).
41. E. Viollier, P. W. Inglett, K. Hunter, A. N. Roychoudhury, P. Van Cappellen, The ferrozine method revisited: Fe(II)/Fe(III) determination in natural waters. *Appl. Geochem.* **15**, 785–790 (2000).
42. J. D. H. Strickland, T. R. Parsons, *A Practical Handbook of Seawater Analysis*, J. C. Stevenson, Ed. (Fisheries Research Board of Canada, Ottawa, 1972), pp. 77–80.
43. D. Payne *et al*., Geologic legacy spanning >90 years explains unique Yellowstone hot spring geochemistry and biodiversity. *Environ. Microbiol.* **21**, 4180–4195 (2019).
44. G. J. Schut *et al*., The role of geochemistry and energetics in the evolution of modern respiratory complexes from a proton-reducing ancestor. *Biochim. Biophys. Acta* **1857**, 958–970 (2016).
45. D. Søndergaard, C. N. S. Pedersen, C. Greening, D. B. Hyd, HydDB: A web tool for hydrogenase classification and analysis. *Sci. Rep.* **6**, 34212 (2016).
46. M. T. Jones *et al*., Monitoring of jökulhlaups and element fluxes in proglacial Icelandic rivers using osmotic samplers. *J. Volcanol. Geotherm. Res.* **291**, 112–124 (2015).
47. E. S. Boyd *et al*., Diversity, abundance, and potential activity of nitrifying and nitrate-reducing microbial assemblages in a subglacial ecosystem. *Appl. Environ. Microbiol.* **77**, 4778–4787 (2011).
48. P. A. Canovas, "Energy transfer between the geosphere and biosphere," PhD dissertation, School of Life Sciences, Arizona State University, Tempe, AZ (2016).
49. M. J. Amenabar, M. R. Urschel, E. S. Boyd, "Metabolic and taxonomic diversification in continental magmatic hydrothermal systems" in *Microbial Evolution Under Extreme Conditions*, C. Bakermans, Ed. (De Gruyter, Berlin, 2015), chap. 4, pp. 57–95.
50. F. Klein, N. G. Grozeva, J. S. Seewald, Abiotic methane synthesis and serpentinization in olivine-hosted fluid inclusions. *Proc. Natl. Acad. Sci. U.S.A.* **116**, 17666–17672 (2019).
51. M. J. L. Bas, A. L. Streckeisen, The IUGS systematics of igneous rocks. *J. Geol. Soc. London* **148**, 825–833 (1991).
52. P. C. Novelli *et al*., Molecular hydrogen in the troposphere: Global distribution and budget. *J. Geophys. Res. Atmos.* **104**, 30427–30444 (1999).
53. C. Greening *et al*., Persistence of the dominant soil phylum Acidobacteria by trace gas scavenging. *Proc. Natl. Acad. Sci. U.S.A.* **112**, 10497–10502 (2015).
54. M. Tranter, "Sediment and solute transport in glacial meltwater streams" in *Encyclopedia of Hydrological Sciences*, M. G. Anderson, Ed. (Wiley, 2006).
55. B. A. Wiggins, S. H. Jones, M. Alexander, Explanations for the acclimation period preceding the mineralization of organic chemicals in aquatic environments. *Appl. Environ. Microbiol.* **53**, 791–796 (1987).
56. J. Aamand, C. Jørgensen, E. Arvin, B. K. Jensen, Microbial adaptation to degradation of hydrocarbons in polluted and unpolluted groundwater. *J. Contam. Hydrol.* **4**, 299–312 (1989).
57. H. Wang, K. J. Edwards, Bacterial and archaeal DNA extracted from inoculated experiments: Implication for the optimization of DNA extraction from deep-sea basalts. *Geomicrobiol. J.* **26**, 463–469 (2009).
58. M. Ji *et al*., Atmospheric trace gases support primary production in Antarctic desert surface soil. *Nature* **552**, 400–403 (2017).
59. M. R. Urschel, T. L. Hamilton, E. E. Roden, E. S. Boyd, Substrate preference, uptake kinetics and bioenergetics in a facultatively autotrophic, thermoacidophilic crenarchaeote. *FEMS Microbiol. Ecol.* **92**, fiw069 (2016).
60. M. J. Amenabar, D. R. Colman, S. Poudel, E. E. Roden, E. S. Boyd, Electron acceptor availability alters carbon and energy metabolism in a thermoacidophile. *Environ. Microbiol.* **20**, 2523–2537 (2018).
61. C. R. Carere *et al*., Mixotrophy drives niche expansion of verrucomicrobial methanotrophs. *ISME J.* **11**, 2599–2610 (2017).
62. J. Foght *et al*., Culturable bacteria in subglacial sediments and ice from two Southern Hemisphere glaciers. *Microb. Ecol.* **47**, 329–340 (2004).
63. P. M. Wynn, A. Hodson, T. Heaton, Chemical and isotopic switching within the subglacial environment of a high Arctic glacier. *Biogeochemistry* **78**, 173–193 (2006).
64. H. R. Beller *et al*., The genome sequence of the obligately chemolithoautotrophic, facultatively anaerobic bacterium *Thiobacillus denitrificans*. *J. Bacteriol.* **188**, 1473–1488 (2006).
65. K. Jónasson, Silicic volcanism in Iceland: Composition and distribution within the active volcanic zones. *J. Geodyn.* **43**, 101–117 (2007).
66. G. R. Robson, *The Volcanic Geology of Vestur–Skaftarfellssysla Iceland* (Durham University, 1956).
67. C. M. Hansel *et al*., Dominance of sulfur-fueled iron oxide reduction in low-sulfate freshwater sediments. *ISME J.* **9**, 2400–2412 (2015).
68. K. Kashefi *et al*., *Geoglobus ahangari* gen. nov., sp. nov., a novel hyperthermophilic archaeon capable of oxidizing organic acids and growing autotrophically on hydrogen with Fe(III) serving as the sole electron acceptor. *Int. J. Syst. Evol. Microbiol.* **52**, 719–728 (2002).
69. K. Kashefi, D. E. Holmes, A.-L. Reysenbach, D. R. Lovley, Use of Fe(III) as an electron acceptor to recover previously uncultured hyperthermophiles: Isolation and characterization of *Geothermobacterium ferrireducens* gen. nov., sp. nov. *Appl. Environ. Microbiol.* **68**, 1735–1742 (2002).

70. P. R. Norris *et al*., *Acidithiobacillus ferrianus* sp. nov.: An ancestral extremely acidophilic and facultatively anaerobic chemolithoautotroph. *Extremophiles* **24**, 329–337 (2020).
71. R. Margesin, D.-C. Zhang, D. Frasson, A. Brouchkov, *Glaciimonas frigoris s*p. nov., a psychrophilic bacterium isolated from ancient Siberian permafrost sediment, and emended description of the genus *Glaciimonas*. *Int. J. Syst. Evol. Microbiol.* **66**, 744–748 (2016).
72. D. Frasson *et al*., *Glaciimonas alpina* sp. nov. isolated from alpine glaciers and reclassification of *Glaciimonas immobilis* Cr9-12 as the type strain of *Glaciimonas alpina* sp. nov. *Int. J. Syst. Evol. Microbiol.* **65**, 1779–1785 (2015).
73. D.-C. Zhang, M. Redzic, F. Schinner, R. Margesin, *Glaciimonas immobilis* gen. nov., sp. nov., a member of the family Oxalobacteraceae isolated from alpine glacier cryoconite. *Int. J. Syst. Evol. Microbiol.* **61**, 2186–2190 (2011).
74. O. Lenz, M. Bernhard, T. Buhrke, E. Schwartz, B. Friedrich, The hydrogen-sensing apparatus in *Ralstonia eutropha*. *J. Mol. Microbiol. Biotechnol.* **4**, 255–262 (2002).
75. J. L. Darcy, R. C. Lynch, A. J. King, M. S. Robeson, S. K. Schmidt, Global distribution of *Polaromonas* phylotypes—evidence for a highly successful dispersal capacity. *PLoS One* **6**, e23742 (2011).
76. A. Hiraishi, J. F. Imhoff, "Rhodoferax" in *Bergey's Manual of Systematics of Archaea and Bacteria* (American Cancer Society, 2015), pp. 1–11.
77. Y. Liu *et al*., A trans-outer membrane porin-cytochrome protein complex for extracellular electron transfer by *Geobacter sulfurreducens* PCA. *Environ. Microbiol. Rep.* **6**, 776–785 (2014).
78. L. Shi, J. K. Fredrickson, J. M. Zachara, Genomic analyses of bacterial porin-cytochrome gene clusters. *Front. Microbiol.* **5**, 657 (2014).
79. L. Shi, K. M. Rosso, J. M. Zachara, J. K. Fredrickson, Mtr extracellular electron-transfer pathways in Fe(III)-reducing or Fe(II)-oxidizing bacteria: A genomic perspective. *Biochem. Soc. Trans.* **40**, 1261–1267 (2012).
80. G. F. White *et al*., Rapid electron exchange between surface-exposed bacterial cytochromes and Fe(III) minerals. *Proc. Natl. Acad. Sci. U.S.A.* **110**, 6346–6351 (2013).
81. K. T. Finneran, C. V. Johnsen, D. R. Lovley, *Rhodoferax ferrireducens* sp. nov., a psychrotolerant, facultatively anaerobic bacterium that oxidizes acetate with the reduction of Fe(III). *Int. J. Syst. Evol. Microbiol.* **53**, 669–673 (2003).
82. P. F. Hoffman, A. J. Kaufman, G. P. Halverson, D. P. Schrag, A neoproterozoic snowball Earth. *Science* **281**, 1342–1346 (1998).
83. S. Hotaling, E. Hood, T. L. Hamilton, Microbial ecology of mountain glacier ecosystems: Biodiversity, ecological connections and implications of a warming climate. *Environ. Microbiol.* **19**, 2935–2948 (2017).
84. E. Garcia-Lopez, C. Cid, Glaciers and ice sheets as analog environments of potentially habitable icy worlds. *Front. Microbiol.* **8**, 1407 (2017).
85. J. H. Waite *et al*., Cassini finds molecular hydrogen in the Enceladus plume: Evidence for hydrothermal processes. *Science* **356**, 155–159 (2017).